Numerical Propeller Rudder Interaction Studies to Assist Fuel Efficient Shipping

Charles Badoe[1*], *Alexander Phillips*[1] and *Stephen R Turnock*[1]

[1] Faculty of Engineering and the Environment, University of Southampton, Southampton, UK
Email: cb3e09@soton.ac.uk

** corresponding author*

Abstract

Reducing the fuel consumption of shipping presents opportunities for both economic and environmental gain. From a resistance and propulsion standpoint, a more holistic propeller/hull/rudder interaction strategy has the potential to reduce fuel consumption, and minimise the risk of cavitation. The goal of this paper is to demonstrate that powering requirements can be reduced by optimizing the interaction between a ship's rudder and propeller. In this paper, ongoing investigation regarding the design of an energy efficient rudder by adapting the local rudder incidence across the span to the effective inflow angle due to propeller swirl is presented. Numerical simulations are performed using an open-source RANS CFD code, Open FOAM, due to its ease with complex topology. Propeller effects are simulated using a body force model approach with special emphasis on ensuring the correct inflow to the rudder.

Keywords: Rudder, Propeller, Maritime, Emissions

1. Introduction

Reducing the fuel consumption of shipping presents opportunities for both economic and environmental gain. The goal of this paper is to demonstrate that ship powering requirements can be reduced by optimizing the interaction between a ship's rudder and propeller. Extensive research and investigations into the complex flow phenomena that exist between the propeller and rudder have been performed, Molland and Turnock (1991) conducted wind tunnel investigations on the influence of propeller loadings on a series of rudder geometries. The tests highlighted the distribution of loading over rudder through measurements of rudder forces, moments and pressure distribution. Simonsen (2000) investigated the flow field around a propeller-rudder and hull combination using Reynolds Averaged Navier Stokes (RANS) simulations. Bertram (2009) investigated the problem of the propeller-induced perturbation on the rudder. The study aimed at providing insights on the key mechanisms governing the complex interaction between the propeller wake structures and the rudder. Important flow features distinguishing flow field around a rudder operating in the race of a propeller were highlighted examples of which are the complex dynamics of propeller tip vortices and the re-storing mechanism of the tip vortex downstream of the rudder. Phillips et al. (2010) also investigated the interaction between the propeller and rudder using a commercial RANS code the influence of the propeller on the flow was modelled using three body force propeller models. They developed an iterative meshing approach which allows good capture of extents of propeller race downstream of the rudder and the vortical structures.

In this paper, a method for rapidly computing the flow field and integrated forces acting on a rudder in a propeller race is presented. An open source RANS code is used for the investigation, propeller effects are simulated using a body force model approach with special emphasis on ensuring the

correct inflow to the rudder. In order to systematically investigate the problem, a series of numerical experiments are presented for

(a) A 3-D rudder in free stream conditions

(b) A propeller-rudder combination operating in open water, results of which are compared with wind tunnel experiments by Molland and Turnock (2007).

(c) Finally a twisted rudder geometry is considered, which reduces rudder drag.

2. Computational Tool

The open source CFD code Open FOAM (Open Field Operation and Manipulation) was used for the investigation. It solves the Reynolds Averaged Navier Stokes (RANS) equations using a cell-centered finite-volume method. The RANS equations can be written in the form:

$$\frac{\partial \overline{U_i}}{\partial x_i} = 0 \tag{1}$$

$$\rho \frac{\partial \overline{U_i}}{\partial t} + \rho \frac{\partial \overline{U_i U_j}}{\partial x_j} = -\frac{\partial P}{\partial x_i} + \frac{\partial}{\partial x_j}\left\{ \mu \left(\frac{\partial \overline{U_i}}{\partial x_j} + \frac{\partial \overline{U_j}}{\partial x_i} \right) \right\} - \rho \frac{\partial \overline{u'_i u'_j}}{\partial x_j} + f_i \tag{2}$$

The Reynolds stress ($\rho\overline{u'_i u'_j}$) was modelled to close the governing equation by employing a Shear Stress Transport (SST) eddy viscosity turbulence model. The SST k-ω model was developed by Menter (1994) to effectively blend the robust and accurate formulation of the k-ω model in the near-wall region with the free-stream independence of the k-ε model in the far field. Previous investigations using this model has shown to be better at replicating flows involving separation, which is an important issue in the analysis of ship flow, where separation always occurs in the region of ship stern (Gothenburg, 2000).

3. Propeller modeling

The momentum equations include a body force term f_{b_i}, used to model the effects of a propeller without modeling the real propeller. There are several approaches for calculating f_{b_i} including simple prescribed distributions, which recover the total thrust T and torque Q, to more sophisticated methods which require a propeller performance code in an interactive way with the RANS solver to capture propeller rudder interaction and to distribute f_{b_i} according to the actual blade loading. To implement the body force model in OpenFOAM an actuator disk region is defined where the rotor (propeller) is accounted for by adding momentum (volume force) to the fluid (Svenning, 2010). The radial distribution of forces, with components f_{b_x} (axial), f_{b_r}(radial) = 0 and f_{b_θ} (tangential), is based on non-iterative calculation of Hough and Ordway (1964) circulation distribution with optimum type from Goldstein (1929) and without any loading at the root and tip. Stern et al. (1988) coupled this distribution with a RANS simulation and has been implemented in CFDSHIP-IOWA (2003). The non-dimensional thrust distribution f_{b_x} and torque distribution f_{b_θ} are:

$$f_{b_x} = A_x r^* \sqrt{1 - r^*} \tag{3}$$

$$f_{b_\theta} = A_\theta \frac{r^* \sqrt{1 - r^*}}{r^*(1 - r'_h) + r'_h} \tag{4}$$

Where

$$A_x = \frac{C_T}{\Delta} \frac{105}{16(4 + 3r'_h)(1 - r'_h)} \tag{5}$$

$$A_\theta = \frac{K_Q}{\Delta J^2} \frac{105}{\pi(4+3r'_h)(1-r'_h)} \quad (6)$$

and the non-dimensional radius is defined as $r^* = r^* = \frac{r^*-r'_h}{1-r'_h}, r'_h = \frac{R_H}{R_P}, r^* = \frac{r}{R_P}$

$$C_T = \frac{2T}{\rho U^2 \pi {R_P}^2} \quad (7)$$

R_H - *Radius of hub*
R_P - *Radius of propeller*
K_Q - *Torque coefficient*
K_T - *Thrust coefficient*
T - *Thrust*
Δ - *mean chord length projected into the x-z plane (or actuator disk thickness),*
J - Advance coefficient

4. Experimental Data

The cases considered are based on wind tunnel test performed by Molland and Turnock (1991, 1995 and 2007) in the University of Southampton 3.5m x 2.5m RJ Mitchell Wind Tunnel, www(2012). The experimental set-up comprises of a 1m span 1.5 geometric aspect ratio rudder based on NACA 0020 aerofoil section (rudder Nos 2). The propeller is 0.8m diameter and based on the Wageningen B4.40 series. The rudder geometry and its arrangement with respect to the propeller are given in Figure 1, the rudder is positioned at X/D = 0.39.

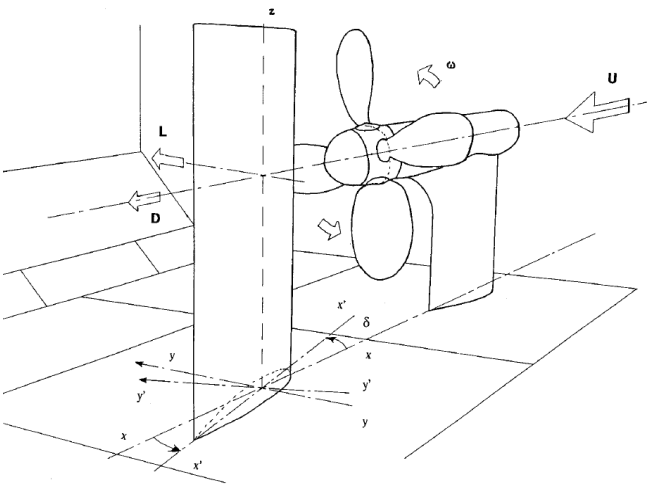

Figure 1: Rudder geometry and its arrangement in respect to propeller
Source: Molland and Turnock (2007)

5. Numerical Model/Mesh Technique

The computational domain matched that of the RJ Mitchell wind tunnel, extending 8 rudder chord lengths upstream of the propeller plane and 12 rudder chord lengths downstream of the rudder trailing edge. The solver settings and simulation parameters can be found in Table 1.

An unstructured hexahedral mesh was created using the SnappyHexMesh utility within OpenFOAM. An initial coarse block mesh was created defining the size of the domain after which specific areas of interest within the domain were then specified for refinement in progressive layers. The total number of grid points was around 2.5 million. Figure 2 shows a cross section grid around the rudder.

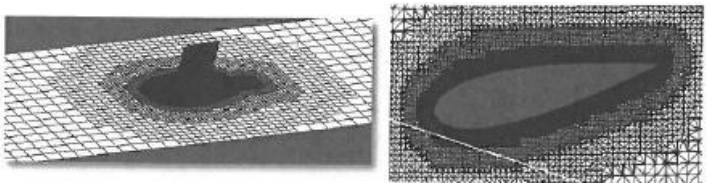

(a) (b)

Figure 2: (a) Tunnel floor &rudder mesh (b) cross section grid around the rudder

Table 1: Numerical model

Parameter	Setting
Mesh Type	Unstructured (Hexahedral)
No. of Elements	Approximately 2.5M
y^+	30
Inlet	Freestream velocity (10m/s)
Outlet	Zero gradient
Tunnel floor/side walls	Slip
Tunnel roof	Slip
Rudder	No Slip
Turbulence model	k- $\boldsymbol{\omega}$ SST Turbulence

6. Results and Discussions

The propeller-rudder combination using rudder No.2 were simulated at 9.6^o, -0.4^o and -10.4^o for a wind speed of 10m/s and Reynolds number of 0.4×10^6. The propeller was fixed at X/D = 0.39 and operates at an advance coefficient of J = 0.35, K_T= 2100 and K_Q= 0.28 Results are presented both for field and integral quantities.

6.1. Lift and Drag data

Figure 3 compares the lift and drag data from the rudder behind a propeller and an earlier investigation conducted for the same rudder in free-stream with experimental data from Molland and Turnock (2007). Results are also presented from Simonsen (2000) and Phillips (2009) who both performed similar investigation using CFDSHIP-IOWA and ANSYS CFX respectively. Simonsen (2000) also presented free stream lift and drag characteristics for a rudder using empirical formulas. These were proposed by Söding (1982) based on potential theory and experiments in Brix (1993). Expressions in appendix 1 are those proposed by Söding (1982). Freestream lift and drag data are also compared with these empirical expressions. Table 2 also compares dCL/dδ.

The results show good agreement at low angles of attack, where the flow is fully attached. There is a considerable increase in lift when the rudder is placed behind a propeller. This is due to the propeller race significantly increasing the inflow velocity to the rudder, see Figure 4.

The computed drag is predicted higher than found in the free-stream rudder. For both the rudder behind a propeller and the free-stream rudder cases the drag coefficient was marginally over-predicted. The over-prediction was higher for the rudder behind a propeller case. This could be due to several factors; first the wall boundary layer at the rudder root was neglected, this may also have contributed to the difference observed in the lift plot. Secondly the over prediction might also be due to frictional drag computation (laminar-turbulent transition). The numerical simulation assumes a fully turbulent boundary layer, while the flow over the experimental rudder was tripped from laminar to turbulent

flow at a distance of 5.7% from the leading edge of the chord on both sides of the rudder using turbulence strips. The problem has been addressed by Hoffman et al (1989) who carried out investigations on "the Influence of Freestream Turbulence on Turbulent Boundary Layers with Mild Adverse Pressure Gradients". They concluded that transition is a very sensitive flow phenomenon and, as such, can be strongly affected by experimental conditions (in particular, the level of freestream turbulence); CFD computations tend to overestimate the drag force.

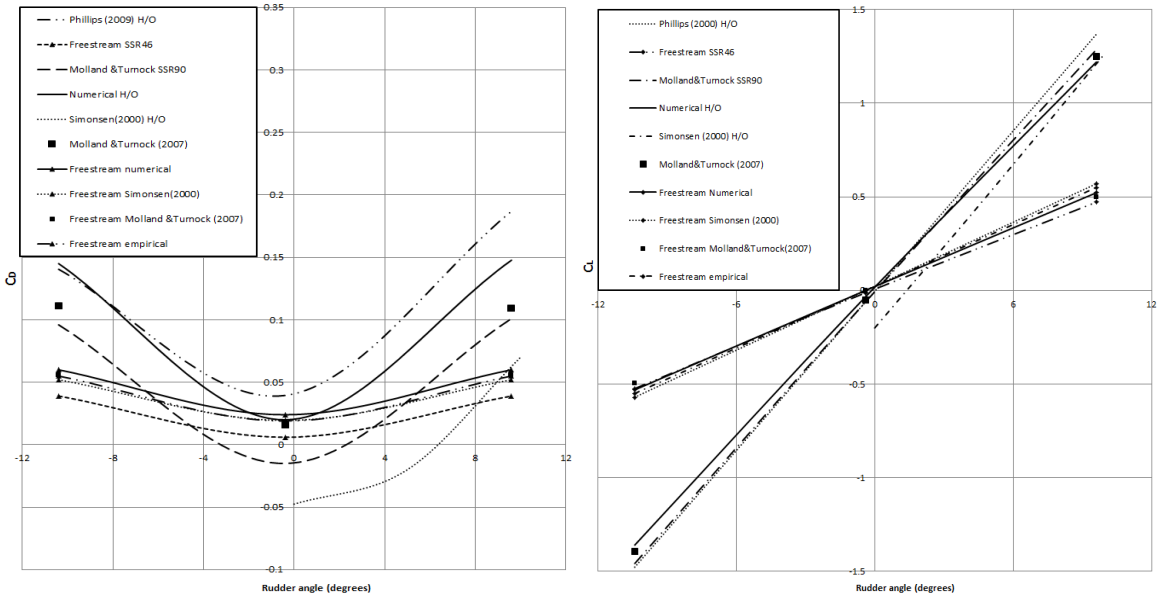

Figure 3: Force data for rudder No.2 freestream (w/o propeller) and with propeller J =0.35

Table 2: Rudder lift performance

Data	$dC_L/d\delta$
Molland &Turnock (2007)	0.132
Molland &Turnock (SSR90)	0.136
Simonsen(2000) H/O	0.147
Phillips(2009) H/O	0.136
Numerical H/O	0.129
Molland &Turnock(freestream rudder)	0.0498
Emipical(freestream rudder)	0.055
Simonsen(2000) (freestream rudder)	0.057
Numerical (freestream rudder)	0.052

6.2. Rudder Surface Pressure Distribution

Pressure distribution around a rudder is an important parameter, both in terms of hydrodynamic characteristics and boundary-layer behaviour. To investigate the performance of the propeller code used for the investigation, pressure distribution was plotted at different spanwise locations on the rudder surface from the root to the tip. Since the inflow velocity to the rudder is greater than freestream accurate determination of the pressure distribution means that the correct inflow velocity to the rudder has been generated by the propeller model. Rudder inflow velocities were plotted and compared with experimental results (Figure 4). The propeller code could not recreate the inflow over the root but areas close to the hub and tip, the inflow velocities were created much better. Figure 5a shows the flow effect in the vicinity of the leading edge of the rudder and 5b&c presents the pressure distribution on the rudder surface as a result of the action of the propeller. Clearly from Figures 5a&b, propeller effects can be observed. Areas of high pressure regions observed close to the leading edge were due to the swirl of the slipstream which makes contact with the lower part of the suction and upper part of the pressure side. Figure 6 also shows the plot of pressure distribution at eight spanwise locations of the rudder from the root to the tip. The computed pressure distribution represented by the

local pressure coefficient C_p is given by: $C_p = \frac{p - p_\infty}{0.5\rho U_\infty^2}$ where $p - p_\infty$ is the local pressure; ρ is the density and U is the free stream velocity. Agreement was good in areas close to the tip Figs (span 940mm &970mm). The slight difference observed was as a result of the tip vortex, which introduces some unsteadiness which could not be captured by the solver. At mid chord (span 530mm; 705mm&880mm) areas close to the hub, pressure distributions were under predicted. The under prediction was due to the fact that the propeller code does not take into account the effect of the hub. Hence flow effect as a result of the hub could not be adequately captured. Since the floor boundary layer was neglected, interaction between the floor and the root could not be modeled. This was evident in the pressure plot for areas close to the root (span 70mm). Simonsen (2000) who performed similar investigation suggested that, if body force is not smoothly distributed around the entire actuator disk region there will be discrepancies between numerical and experimental results hence this was also evident in the results obtained.

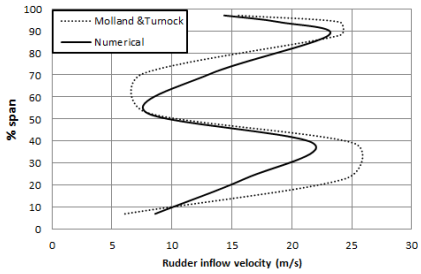

Figure 4: Rudder inflow velocity δ =9.6°

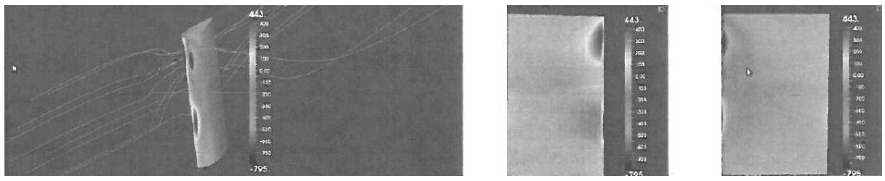

(a) (b) (c)

Figure 5: Pressure distribution on rudder surface δ =9.6° (a) with streamlines (b) pressure side (c) suction side

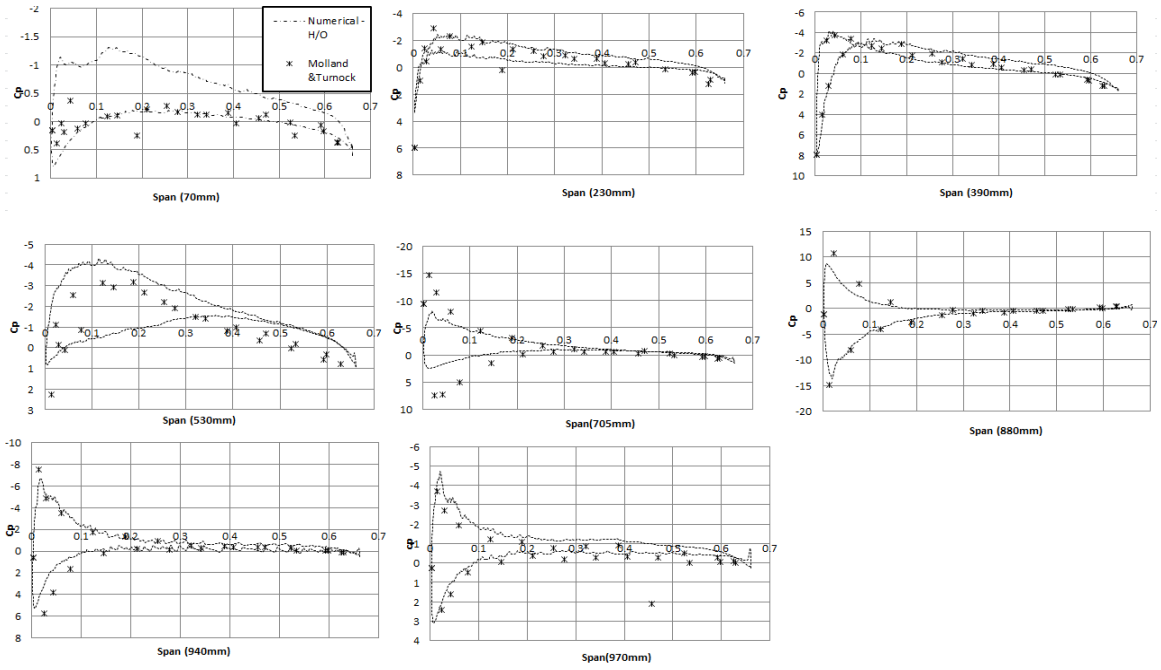

Figure 6: Rudder pressure distribution, J = 0.35 δ =9.6°

7. The Rudder Design

As already discussed, for a rudder operating behind a propeller, the flow to the rudder will have large cross components that vary along the span, due to the swirl component in the propeller race. This results in spanwise variations in local inflow angle to the rudder. To improve rudder operation and minimize cavitation, a twisted rudder design was adopted based on the results presented. The concept behind the twisted rudder is to adapt the local rudder incidence across the span to the effective inflow angle as a result of the rotation of the propeller slipstream. Hence for a rudder at an angle of zero degrees it should have zero effective incidence across the span.

The twisted rudder concept was many years ago, adopted by the United States navy to a surface ship combatant and was found to reduce the problem of cavitation and erosion Shen et al (1997). To determine the twist angle for reducing rudder cavitation inception, an estimate of the inflow angle based on the velocity profile in figure 4 was generated and an initial twist angle curve (line) applied to the rudder.

Figure 7 shows the initial twist angle curve (line) adopted for this work. To determine the effectiveness of the twist, field and integral data were generated for the twisted rudder at -10.4^o, -0.4^o, 9.6^o and compared to results from the straight rudder discussed earlier. Figure 8 shows the lift and drag plot of the straight rudder and the twisted rudder at -0.4^o and 9.6^o incidence. It is clear from the lift plot that the twisted rudder results in a decrease in lift for lower incidence as compared to the straight rudder. This is desirable for manoeuvring purposes. The drag characteristics also show a reduction in drag for the twisted rudder as compared to the straight rudder. The drag difference between straight and twist rudder decreases as the angle of incidence increase. This is because at low incidence there is lower effective incidence and load across the span. Ideally for an angle of attack of zero degrees it is expected to have a zero effective incidence across the span of the rudder. The results presented are for an initial assumed twist angle distribution hence it is desirable to fine tune the twisted angle to obtain an optimum twist distribution for further improvement in lift and drag characteristics.

Figure 9 shows the pressure distribution on the rudder surfaces for straight rudder (left) and twisted rudder (right) at -10.4^o (top); -0.4^o (middle) and 9.6^o (bottom). Both asymmetrical loadings and low and high pressure hotspots are clearly indicated signifying delayed onset of cavitation for a twisted rudder.

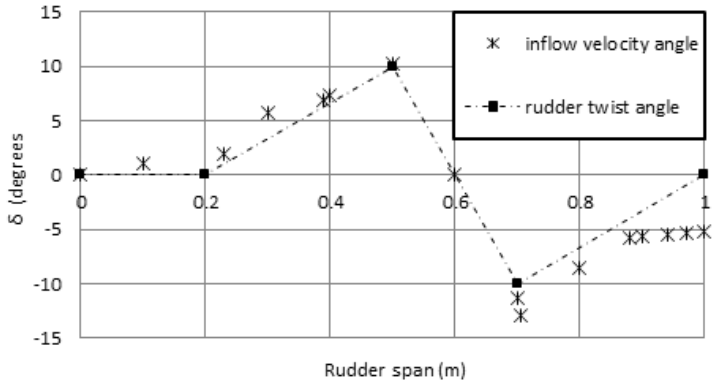

Figure 7: Inflow angle and (adopted) rudder twist angle in the spanwise direction of rudder

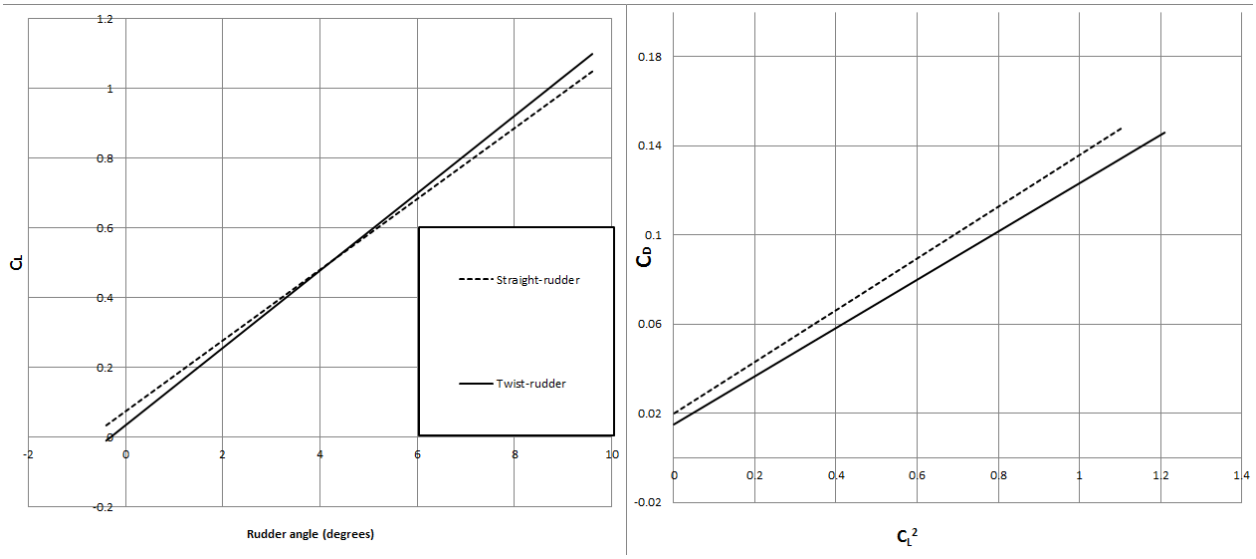

Figure 8: Force data for twist and straight rudder J =0.35

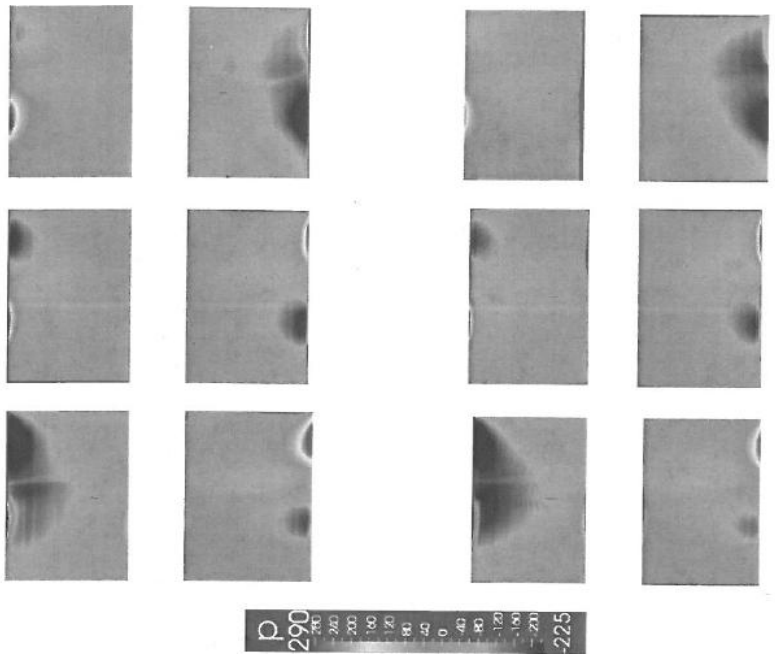

Figure 9: Straight (left) and twist (right) rudder pressure distribution, J = 0.35 $\delta = -10^o$(top); 0^o(middle) & 10^o (bottom).

8. Conclusion

Results of the present work have shown how open source CFD codes can be applied to gain valuable insight into the interaction between the propeller and rudder. The results highlight that simple body force propeller approaches can be quickly and reliably used to predict rudder forces within 10% of experimentally calculated values. Alternative rudder geometries can be quickly generated and assessed to determine appropriate rudder shapes.

The numerical simulations allow easy extraction of the local inflow angles to the rudder, enabling twisted rudder configurations to be rapidly developed based on bespoke inflows. Using an appropriate twisted angle distribution, the rudder drag at zero lift was modified from C_D= 0.020 for a straight rudder to C_D=0.015 for the twisted rudder a reduction of 75%. Additionally by reducing the local inflow angle of the rudder the magnitude of low pressure regions around the rudder are reduced, which should reduce the susceptibility of the rudder to cavitation.

The key limitation of the methodology presented above is the impact of the rudder on the performance of the propeller, which is not considered. Work is ongoing to allow full hull-propeller-rudder interaction studies to be performed so that complete hydrodynamic propulsive efficiency studies can be performed.

9. Acknowledgement

The author acknowledges the use of the IRIDIS High Performance Computing Facility, and associated support services at the University of Southampton in completion of this work.

References

Bertram, V. (2009), "Fuel Saving Options for Ships," Annual Marine Propulsion Conf., London.

Brix J., ed. (1993), Manoeuvring Technical Manual, Seehafan Verlag GmbH, Hamburg, 1993.

CFDSHIP-IOWA, (2003), Hydroscience & Engineering, The University of Iowa100 C. Maxwell Stanley Hydraulics Laboratory Iowa City, Iowa 52242-1585.

Goldstein, S. (1929) "On the Vortex Theory of Screw Propellers", Proc. of the Royal Society (A) 123, 440.

Gothenburg (2000) Workshop, Journal of Ship Research, Vol. 47, No. 1, March 2003, pp. 63–8[15].

Hoffman, J. A., Kassir, S. M., and Larwood, S. M. (1989), "The Influence of Freestream Turbulence on Turbulent Boundary Layers with Mild Adverse Pressure Gradients," NASA CR 177520.

Hough, G. and Ordway, D. (1964), "The Generalized Actuator Disk," Technical Report TARTR 6401, Therm Advanced Research, Inc.

Larsson, L. and Baba, E. (1996), Ship resistance and flow computations. Advances in marine hydrodynamics. Ohkusu 9ed, Comp. Mech. Publ., pp.1-75.

Menter, F. R. (1994), Two-Equation Eddy-Viscosity Turbulence Models for Engineering Applications [J]. AIAA Journal, 32(8):1598-1605.

Molland, A. F. and Turnock, S. R. (1991), Wind tunnel investigation of the influence of propeller loading on ship rudder performance. Technical report, Ship Science Report No. 46.

Molland, A. F. and Turnock, S. R. (1995), Wind tunnel tests on the effect of a ship hull on rudder-propeller performance at different drift angles. Technical report, University of Southampton Ship Science Report No. 76.

Molland, A.F. and Turnock, S.R. (2007), Marine rudders and control surfaces: principles, data, design and applications, Oxford, UK, Butterworth-Heinemann, 386pp.

Phillips, A.B., Turnock, S.R. and Furlong, M.E. (2010) Accurate capture of rudder-propeller interaction using a coupled blade element momentum-RANS approach. Ship Technology Research (Schiffstechnik), 57, (2), 128-139.

Shen, Y.T., Jiang, C. W., and Remmers, K.D. (1997), "A twisted rudder for reduced cavitation", Journal of Ship Research, Vol. 41, No. 4, pp. 260-272.

Simonsen, C. (2000), Propeller – Rudder interaction by RANS. PhD thesis, University of Denmark.

Söding, H. (1982), Prediction of Ship Steering Capabilities, Shiffstechnik, Bd. 29 pp.3-24.

Stern, F., Kim, H.T., Patel, V.C. and Chen, H.C. (1988b), "Computation of Viscous Flow around Propeller-Shaft Configurations," Journal of Ship Research, Vol. 32, No. 4, pp. 263-284.

Svenning, E. (2010), Implementation of an actuator disk in OpenFOAM. Developed for 1.5dev.

University of Southampton website: www.windtunnel.soton.ac.uk/index.html, last accessed in May 2012.

Appendix 1

$C_L = \frac{2\pi \wedge(\wedge+1)}{(\wedge+2)^2} \sin\delta + C_q |sin\ \delta| \cos\delta$

$C_D = 1.1 \frac{{C_L}^2}{\pi \wedge} + C_q |sin\ \delta|^3 C_{D0}$

Where
C_L - lift coefficient
C_D - drag coefficient
$\wedge$ - aspect ratio
C_q - resistance coefficient used for rudders with square tips i.e. sharp ends and is approx.=1
C_{D0} - surface friction given in ITTC as $C_{D0} = \frac{0.075}{(log_{10}Re-2)^2}$